LANGMUIR

Article

pubs.acs.org/Langmuir

Adsorption of DNA Fragments at Aqueous Graphite and Au(111) via Integration of Experiment and Simulation

Zak E. Hughes,[†] Gang Wei,[‡] Kurt L. M. Drew,[†] Lucio Colombi Ciacchi,*[,‡] and Tiffany R. Walsh*[,†]

[†]Institute for Frontier Materials, Deakin University, Geelong, VIC 3216, Australia

[‡]Hybrid Materials Interface Group, Faculty of Production Engineering, University of Bremen, D-28359 Bremen, Germany

Supporting Information

ABSTRACT: We combine single molecule force spectroscopy measurements with all-atom metadynamics simulations to investigate the cross-materials binding strength trends of DNA fragments adsorbed at the aqueous graphite C(0001) and Au(111) interfaces. Our simulations predict this adsorption at the level of the nucleobase, nucleoside, and nucleotide. We find that despite challenges in making clear, careful connections between the experimental and simulation data, reasonable consistency between the binding trends between the two approaches and two substrates was evident. On C(0001), our simulations predict a binding trend of dG > dA ≈ dT > dC, which broadly aligns with the experimental trend. On Au(111), the simulation-based binding strength trends reveal stronger adsorption for the purines relative to the pyrimadines, with dG ≈ dA > dT ≈ dC. Moreover, our simulations provide structural insights into the origins of the similarities and differences in adsorption of the nucleic acid fragments at the two interfaces. In particular, our simulation data offer an explanation for the differences observed in the relative binding trend between adenosine and guanine on the two substrates.

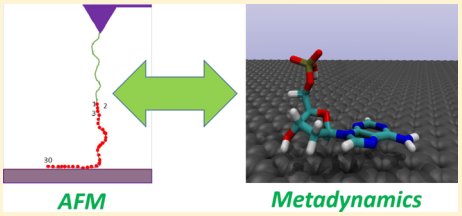

INTRODUCTION

The interactions of biomolecules with inorganic substrates can be exploited in a wide range of applications including biosensing,[1,2] medicine,[3] materials assembly,[4] and more.[5] However, to drive these technologies further, a deeper comprehension of the relationship between the properties of these interfacial systems and the structural traits of the adsorbed biomolecules is required.

Atomic force microscopy (AFM) based single molecule force spectroscopy (SMFS) provides a means by which the adsorption force of a molecule to a substrate may be measured, providing information about these interfacial interactions.[2] By performing SMFS experiments under different conditions, valuable insights into the interactions of the molecule with the substrate can be obtained. For example, recent SMFS experiments were used to measure the force of adhesion of single-stranded (ss) DNA oligomers to graphite substrates.[6,7] It was found that in aqueous solution a ssDNA oligomer would adsorb strongly to the substrate. However, if even small amounts (<1 nmol) of the complementary piece of ssDNA were present in solution, the force required to detach the probe DNA from the graphite substrate was significantly reduced.[7] It was hypothesized that the reason for this reduction in the measured peeling force was due to the hybridization of the two ssDNA strands and that the interaction of the resultant dsDNA with the substrate was significantly weaker than that of ssDNA. However, while changes in the measured forces can be observed via SMFS, it is challenging to relate such differences to specific changes in the structure of the adsorbed biomolecules using experimental techniques alone.

Molecular dynamics (MD) simulations provide an approach by which the structure of biomolecules adsorbed at aqueous interfaces can be investigated, allowing links to be made between the structure of an adsorbed biomolecule(s) and the properties of the system.[8,9] However, one of the challenges that has traditionally limited the ability of MD simulations to elucidate significant insights into biotic/abiotic interfaces has been the ensuring that the force field (FF) used in these simulations can describe the interaction of the biomolecule with the aqueous substrate appropriately. To overcome this limitation, several recently developed FFs have been specifically parametrized to capture the interactions of biomolecules with metallic[10−12] and graphitic surfaces.[13] However, a general lack of comprehensive experimental data available for comparison with molecular simulation, such as the free energy of adsorption of small molecules, means that the validation, and systematic improvement, of these FFs remains a major challenge.

Experimental techniques such as quartz crystal microbalance (QCM) measurements and surface plasmon resonance (SPR) spectroscopy offer an approach for determining the free energy of adsorption of biomolecules to substrates.[14,15] In principle, these free energies could be compared against those obtained from MD simulations, which would provide a valuable point of verification for biointerfacial FFs. In practice, however, determination of the free energy of adsorption of large biomolecules, such as peptides or ssDNA oligomers using MD simulations, while possible,[16−19] is extremely challenging,

Received: July 18, 2017
Revised: September 6, 2017
Published: September 8, 2017

DOI: 10.1021/acs.langmuir.7b02480
Langmuir 2017, 33, 10193−10204

and can be associated with significant uncertainties, as well as being computationally expensive. On the other hand, the determination of the free energy of small biomolecules, such as amino acids (AAs) or nucleic acids (NAs), from molecular simulation is more practicable.[12,20] However, in contrast, QCM or SPR measurements on such small molecules can be challenging, and therefore there is a gap between simulation and experiment in terms of the calculation of free energies of adsorption of molecules to aqueous interfaces. SMFS measurements, in partnership with MD simulations, is a plausible strategy to overcome this obstacle.

By combining molecular simulation with experimental SMFS measurements, we seek to make connections between experiment, theory, and simulation, providing mutual support for each. In the present work, SMFS measurements of homo-oligomeric ssDNA adsorbed at both the aqueous single-crystal Au(111) and C(0001) interfaces have been performed at different pulling rates. Using theoretical models, the measured forces have been used to estimate the free energy of adsorption per nucleotide at these two substrates. These free energy values are compared against those obtained from metadynamics[21] (MetaD) simulations of the nucleobases, nucleosides, and nucleotides to the aqueous Au(111) and C(0001) interfaces. Overall, we find reasonable agreement in the trends between the experimental and computational results, providing validation for both.

METHODS

Experiments. *Materials.* A highly oriented pyrolytic graphite (HOPG) wafer with ZYB quality (10 × 10 mm^2) was purchased from NT-MDT (Moscow, Russia). Single-crystal Au(111) substrate (diameter of 10 mm, purity 99.999%, orientation accuracy of <0.1°, and roughness <0.01 μm) was purchased from MaTecK GmbH (Jülich, Germany). Nonconductive Si_3N_4 AFM probes (DNP-S10) coated with a 45 ± 10 nm thick Ti/Au layer on the back side were obtained from Bruker Corporation (France). Poly-ssDNA with 30 contiguous base sequences (A_{30}, T_{30}, G_{30}, and C_{30}) was synthesized by IBA (Göttingen, Germany). Both 3-aminopropyltriethoxysilane (APTES) and triethoxy(ethyl)silane (TEES) were provided by the Sigma-Aldrich (Germany). The PEG-NHS linker (α-succinimidyl-oxysuccinyl-ω-succinimidyloxysuccinyloxy, polyoxyethylene, M_w = 3400) was obtained from NOF (Belgium).

Modification of AFM Tip. The modification of the AFM tip was performed according to our recent report.[22] First, all of the AFM probes were cleaned in a freshly prepared piranha solution (H_2SO_4:30% H_2O_2 = 7:3) for 30 min to remove the adsorbed organic contaminants on the probes and then washed with ultrapure water and ethanol (98%) for several times. After that, the cleaned AFM probes were immersed into a mixed solution of APTES and TEES (1% in toluene, 1:4, v/v) for 20 min. After washing with ethanol and ultrapure water, the saline-modified AFM probes were transferred into the PEG-NHS linker solution (0.1 mg mL^{-1}) for 1.5 h to tether the linker to the AFM probe. Finally, the washed AFM probes were incubated with poly-ssDNA solution (0.1 μM) for 1 h to bind the DNA molecules onto the AFM probes. The modified probes were washed with a large amount of water to remove any noncovalently adsorbed DNA molecules prior to the SMFS experiments.

AFM probe cantilevers with a nominal spring constant of 0.32 N m^{-1} were used for all of the SMFS experiments. All force−distance (FD) curves were acquired on a NanoWizard 3 NanoScience atomic force microscope (JPK Instruments AG, Germany) in liquid cell with the "Force Spectroscopy" or "Force Mapping" modes. For the Force Mapping mode, each data set was composed of 256 (16 × 16) individual FD curves taken over a 1 × 1 μm^2 area. For the dynamic force spectroscopy experiments, the pulling velocity of the cantilever was adjusted from 0.05 to 5 μm s^{-1} to vary the applied loading rates.

Data Analysis. All of the FD data were analyzed with the JPK SPM Data processing software (Version 5.1.8). For the statistical analysis, all data were expressed as means ± standard deviation (SD) for $n > 40$. Here, n represents the number of data being analyzed, i.e., the actual number of force−displacement curves that presented clear desorption plateaus and could be used for the histogram analysis of the desorption forces. The statistical analysis was conducted with the Origin 8 (version 8.1) at a confidence level of 95%.

Calculation of the Experimental Adsorption Free Energy. Previously, we estimated the adsorption free energy of a polypeptide adsorbed at the aqueous amorphous SiO_2 interface by using both MD simulation and SMFS experiments.[18] We found that the estimation of the experimental adsorption free energy can be achieved by a two-step data processing. In the first step, all of the force data vs loading rate were fitted with the Friddle−Noy−De Yoreo model to obtain the equilibrium force, F_{eq}. Following this, the adsorption free energy (ΔFE_{ads}) can be inferred by using the classic Bell−Evans model, in which the ΔFE_{ads} is defined using the following equations:

$$\Delta FE_{ads} = \frac{F_{eq}^{\ 2}}{2K_{eff}} \tag{1}$$

$$K_{eff} = \frac{K_C K_{PEG}}{K_C + K_{PEG}} \tag{2}$$

where the ΔFE_{ads} is the adsorption free energy, F_{eq} is the equilibrium force obtained from the fitting, K_{eff} is the effective spring constant of the cantilever and PEG-NHS linker, K_c is the spring constant of tip, and K_{PEG} is the stiffness of the linker (full details are provided in section "Calculation of Stiffness of PEG-NHS Linker" and Figure S1 in the Supporting Information). The spring constant of each used tip was determined individually by means of the thermal noise method.[23] With the values of F_{eq}, K_c, and K_{PEG} known, the ΔFE_{ads} of the four ssDNA oligomers with the aqueous C(0001) and Au(111) interfaces are determined by the above two equations.

Simulation Details. The free energy of adsorption of the relevant NAs to C(0001) and the Au(111) surface under aqueous conditions was predicted using well-tempered metadynamics simulations.[21] In our modeling work we used the graphene substrate. We remark that the chief distinctions between graphite and graphene as a substrate lie in the areas of their mechanical (e.g., flexibility) and electronic (e.g., transport) properties, not the adsorption properties, unless e.g. the graphene is supported on another crystalline substrate (which in this case the support can exert a major effect on adsorption) or when it is used in field-effect transistor architectures and placed under a bias potential, etc. This means, as a substrate for noncovalent adsorption, we expect very little difference in the adsorption free energies between the graphite and graphene substrates. Accordingly, our GRAPPA force field would predict very similar adsorption energies on graphite versus graphene. Previous work has shown that while not necessarily providing a definitively exhaustive description, the substrate models used in our simulations provide an acceptable approximation of the C(0001) and Au(111) interfaces.[11,13,19,24,25] The free energies were calculated for the four naturally occurring DNA bases—adenine, cytosine, guanine, and thymine—at the nucleobase, nucleoside, and nucleotide level. The CHARMM29 FF parameters[26] were used to model these molecules, and the modified version of TIP3P,[27,28] compatible with the CHARMM FF, used to model liquid water. The interactions between the nucleic acids and the solvent with the substrates were described using the polarizable GolP-CHARMM[11] and GRAPPA[13] FFs for Au(111) and C(0001), respectively.

For the Au(111) substrate, a gold slab measuring 58.6 × 60.9 Å and five atoms thick was used. These systems were modeled in liquid water, each system containing ∼4900 water molecules and with the periodic distance between Au surfaces of ≈44 Å. For C(0001), each system consisted of two graphene sheets 44.27 × 38.34 Å, separated by 48 Å of liquid water and 36 Å of vacuum. Each system contained 2546 water molecules. For the C(0001) interface, we considered two different solvent environments: liquid water (with a single Na^+ as a counterion for the nucleotides) and 0.16 mol kg^{-1} NaCl solution. For

DOI: 10.1021/acs.langmuir.7b02480
Langmuir 2017, 33, 10193−10204

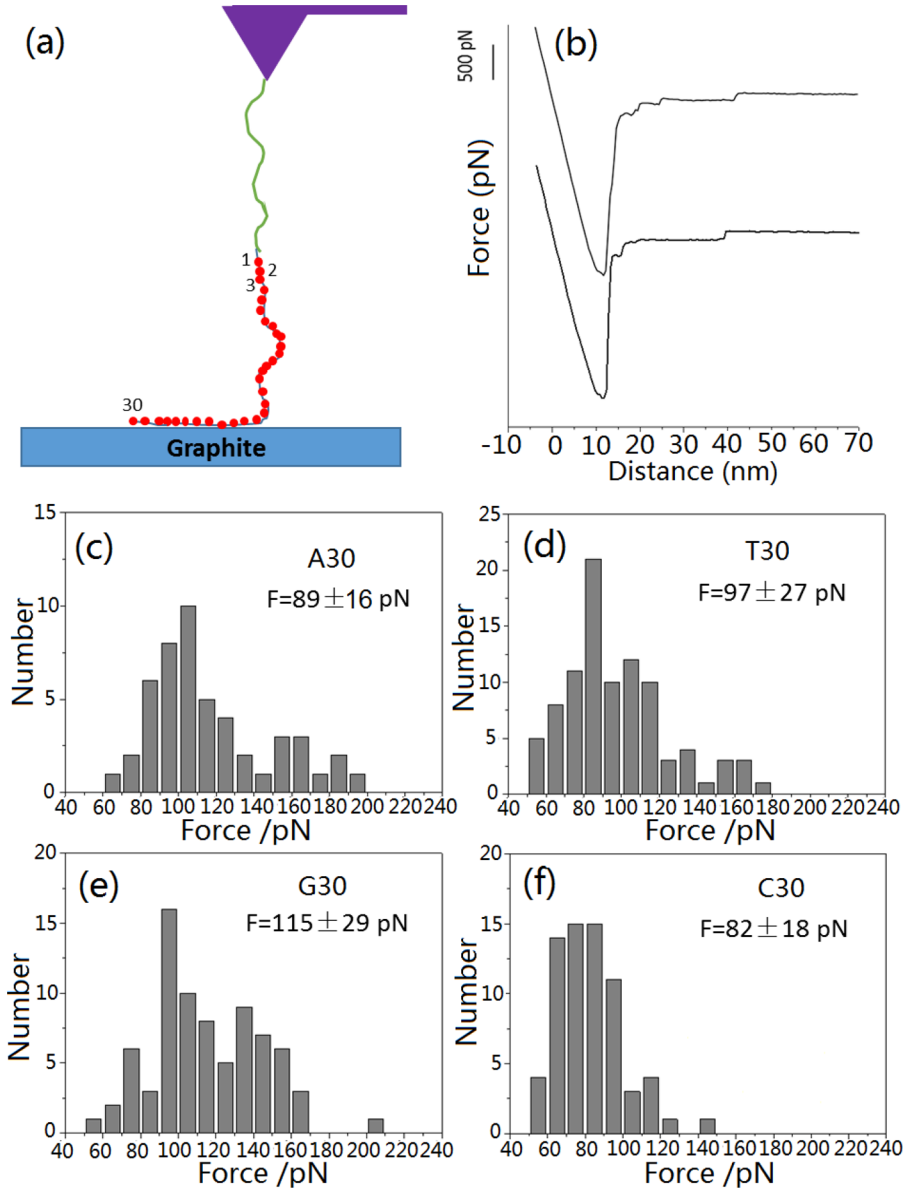

Figure 1. SMFS experiments by peeling 30 base-ssDNA from the aqueous C(0001) interface. (a) Schematic presentation of pulling; (b) typical FD curves. (c–f) Desorption force distributions by peeling: (c) A_{30}, (d) T_{30}, (e) G_{30}, and (f) C_{30} with a pulling velocity of 0.5 μm/s.

both the graphene and Au interfaces, the number of water molecules in the system was such to yield a bulk density of water in the center of the interslab space equivalent to that of a simulation cell of bulk water at the same ambient temperature and pressure.

The simulations were performed using GROMACS version 4.5.5.[29] with version 1.3 of the PLUMED plugin.[30] The Lennard-Jones (LJ) nonbonded interactions were smoothly tapered to zero between 10 and 11 Å, and the electrostatic interactions were evaluated using a particle-mesh Ewald summation,[31] with a real space cutoff of 13 Å. The simulations were performed in the canonical (*NVT*) ensemble, with the temperature maintained at 300 K through the use of the Nosé–Hoover thermostat,[32,33] with a coupling constant of 0.2 ps. In all simulations the collective variable upon which the bias was applied was the position of the center of mass of the nucleobase ring along the *z*-axis (i.e., the direction perpendicular to the substrate surface). Gaussians of 0.5 Å width were deposited every 1 ps, for a total simulation time of 150 ns for the nucleobases, and 350 ns for the nucleosides and nucleotides. The initial Gaussian height was set to 0.2 kJ mol^{-1}, and a well-tempered metadynamics bias factor of 10 was used.

From the free energy profiles, the free energy of adsorption of the adsorbates to the surface was calculated using

$$\Delta FE_{ads} = -k_B T \ln \frac{c_{ads}}{c_{bulk}} \quad (3)$$

where c_{ads} and c_{bulk} are the concentrations of the adsorbate in the surface-adsorbed and bulk states, respectively. These concentrations were calculated as

$$c_{z_0 \to z_1} = \frac{1}{z_1 - z_0} \int_{z_0}^{z_1} \exp(-FE(z)/k_B T)\, dz \quad (4)$$

where z_0 and z_1 are the limits of region in question. In the current work the adsorbed states were defined as those regions within 15 Å of the substrate interface, with the bulk region defined as the remaining space. The final free energies of adsorption were then calculated by averaging over the last 50 or 100 ns of simulation time for the nucleobases and nucleosides/nucleotides, respectively. The uncertainties were estimated from the standard deviation over the same time period.

DOI: 10.1021/acs.langmuir.7b02480
Langmuir 2017, 33, 10193–10204

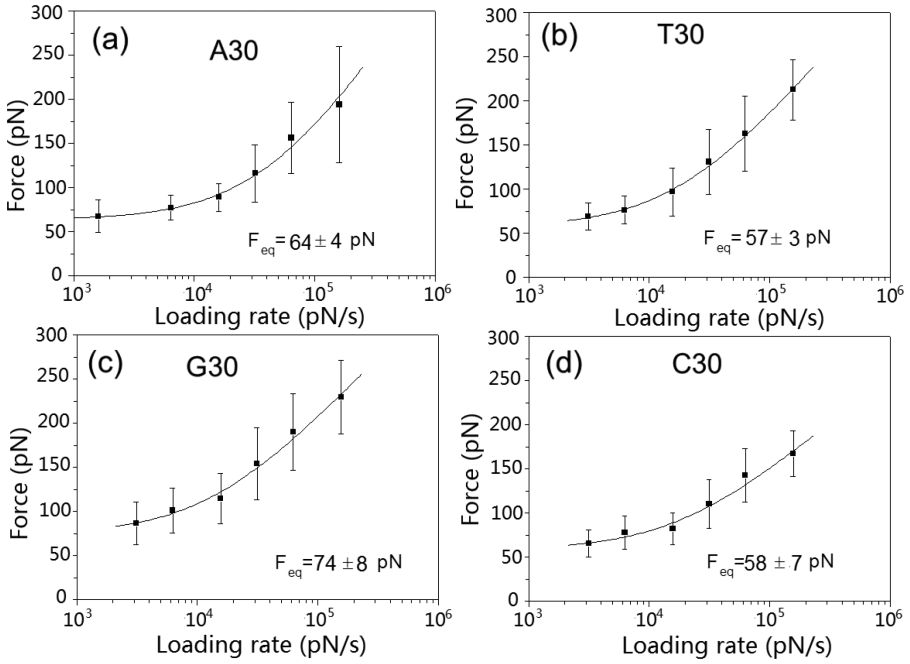

Figure 2. Dynamic force spectroscopy experiments by pulling (a) A_{30}, (b) T_{30}, (c) G_{30}, and (d) C_{30} from aqueous C(0001) with different loading rates. The force at equilibrium state (F_{eq}) was obtained by fitting the force data with the Friddle–Noy–De Yoreo model.

The geometries of the adsorbates were analyzed from the portions of the trajectory where the adsorbate was within ±0.15 Å of the position of the minimum in the free energy profile. The tilt angle of the nucleobase was determined from the angle between the plane of the ring of the nucleobase and plane of the surface. The orientation of the sugar ring was calculated from the angle between a vector normal to the surface and a vector from the center of mass of the ribose ring to the O4 atom. The distances from the surface of the center of mass of the sugar ring and phosphorus atom were also calculated.

RESULTS AND DISCUSSION

Experiments. In this study, we utilized freshly cleaved graphite and single-crystal Au(111) as surfaces for the SMFS experiments. Figure S2 shows typical AFM images of the two surfaces. The corresponding section analysis indicates that their surface roughness within a scan area of 1 × 1 μm^2 was 0.23 ± 0.05 and 1.30 ± 0.24 nm, respectively.

First, we measured the desorption force of the four DNA oligomers (A_{30}, T_{30}, G_{30}, and C_{30}) from C(0001). In this experiment the DNA oligomers were bound onto the AFM tip by a flexible PEG-NHS linker, which can enable them to interact with the C(0001) surface with sufficient conformational freedom. Figure 1b shows typical FD curves. The first strong peak is caused by the van der Waals interaction between the AFM tip and C(0001), whereas the subsequent force plateau is ascribed to the steady-state desorption of ssDNA oligomers. Assuming that interactions among the nucleotides do not significantly affect the force during their progressive desorption, the height of the plateau can be interpreted as the force required to pull individual nucleotides off the surface.[34,35] Figures 1c–f present the measured distributions of desorption forces obtained at a pulling speed of 0.5 $\mu m\ s^{-1}$.

The same measurement was repeated at various pulling speeds in order to assess the variation of the desorption forces with the loading rate. Here, the loading rate was defined as the product between the bending stiffness and the pulling velocity of the AFM tip. Figure 2 shows the obtained results, where it can be seen that the mean desorption force of all ssDNA oligomers increases with the loading rate. These data can then be fitted with the model of Friddle, Noy, and De Yoreo,[36] from which the equilibrium desorption forces and free energies of adsorption of the homo-oligonucleotides can be estimated as described in the Methods section (Table 1). Analogous SMFS experiments were performed to measure the desorption force of the four ssDNA oligomers from the aqueous Au(111) interface. The corresponding results are reported in Figure S3a,b, and all measured values are summarized in Table 1. These data indicate that the ΔFE_{ads} values for the oligomers at the two interfaces are markedly different only in the case of G_{30}, which adsorbed more strongly to the smoother C(0001) interface. Naively, one might expect that the greater roughness of the Au(111) may result in stronger binding at this interface. However, both the nature of the interaction between the nucleobases and the substrate and the possible intramolecular interactions within the oligomer (*vide infra*) may counteract any possible effects arising from the surface roughness.

Table 1. Measured Desorption Forces F_{eq} and Estimated Free Energy of Adsorption ΔFE_{ads} of ssDNA Oligomers from C(0001) and Au(111); K_c Is the Cantilever Stiffness and K_{eff} the Stiffness of the Cantilever/Linker System in Each Case

substrate	DNA oligomer	F_{eq} (pN)	K_c (pN nm^{-1})	K_{eff} (pN nm^{-1})	ΔFE_{ads} (kJ mol^{-1})
C(0001)	A_{30}	64 ± 4	477	32	38 ± 5
	T_{30}	57 ± 3	342	31	32 ± 3
	G_{30}	74 ± 8	342	31	53 ± 11
	C_{30}	58 ± 7	368	31	33 ± 8
Au(111)	A_{30}	61 ± 9	359	31	36 ± 11
	T_{30}	47 ± 8	391	31	21 ± 7
	G_{30}	55 ± 3	299	31	29 ± 3
	C_{30}	54 ± 2	291	30	28 ± 2

DOI: 10.1021/acs.langmuir.7b02480
Langmuir 2017, 33, 10193–10204

Metadynamics Simulations. Table 2 summarizes the free energies of adsorption for all the DNA fragments to the aqueous C(0001) and Au(111) interfaces. Figure 3 shows the free energy profiles and convergence of the free energy as a function of simulation time for guanine, as an exemplar case, at the Au(111) and C(0001) interfaces. The evolution of the free energies as a function of time and free energy profiles for all the different systems are shown in the Supporting Information, Figures S5−S7 and S8−S11, respectively.

Table 2. Free Energies of Adsorption of the DNA Fragments to the Substrates in Aqueous Solution Determined from Metadynamics Simulations

		ΔFE_{ads} (kJ mol^{-1})		
surface	species	nucleobase	nucleoside	nucleotide
C(0001)	A	−22.5 ± 1.0	−25.2 ± 2.1	−27.1 ± 2.5
	C	−12.9 ± 0.9	−18.0 ± 2.5	−21.4 ± 1.0
	G	−27.7 ± 1.6	−31.5 ± 1.7	−38.3 ± 2.0
	T	−16.5 ± 1.0	−23.1 ± 1.6	−27.9 ± 1.7
Au(111)	A	−35.4 ± 1.8	−39.4 ± 1.8	−45.7 ± 3.1
	C	−18.5 ± 1.0	−26.8 ± 1.7	−34.9 ± 1.3
	G	−34.6 ± 1.1	−38.1 ± 0.9	−44.4 ± 1.3
	T	−18.3 ± 0.5	−21.8 ± 0.9	−28.6 ± 1.5

At the aqueous C(0001) interface, by 150 ns of metadynamics simulations the free energy of the nucleobases had converged, as indicated in Figure 3a and Figure S5. The free energy profiles (Figure 3b and Figure S8) exhibit a sharp minimum ∼3.8 Å from the surface and a local minimum located approximately 7 Å from the surface. There is a small barrier between the two minima, which we ascribe to the displacement of the first layer of interfacial water adsorbed at the aqueous interface (similar structuring was observed for the adsorption of amino acids at the aqueous C(0001) interface[24]). All of the nucleobases showed a strong binding affinity to the C(0001) interface, with the free energies of adsorption ranging from −13 to −30 kJ mol^{-1}. The rank ordering of the binding affinities for the nucleobases to C(0001) under aqueous conditions was predicted to be G > A > T > C. This is the same rank ordering predicted by first-principles[37] and FF calculations (summarized in Table S1 of the Supporting Information) for the adsorption of the nucleobases to C(0001) in *in vacuo*.

The addition of the deoxyribose sugar ring had a non-negligible effect on the free energy profiles (Figure 3b and Figure S9). While the position of the global minimum was unchanged, the profile was much deeper (∼−5 kJ mol^{-1}) at a distance 5−10 Å from the C(0001) surface. These changes in the free energy profiles produced an increase in the absolute values of the free energy of adsorption of the nucleosides compared to the nucleobases. Compared against the nucleobases, the rank ordering in the binding affinities of the nucleosides was altered. While G and C were still the strongest and weakest adsorbing species, respectively, the difference between A and T was diminished, such that their binding free energies no longer differed significantly.

The more complex potential energy landscape (PEL) of the adsorbed nucleotides made it more challenging to converge the

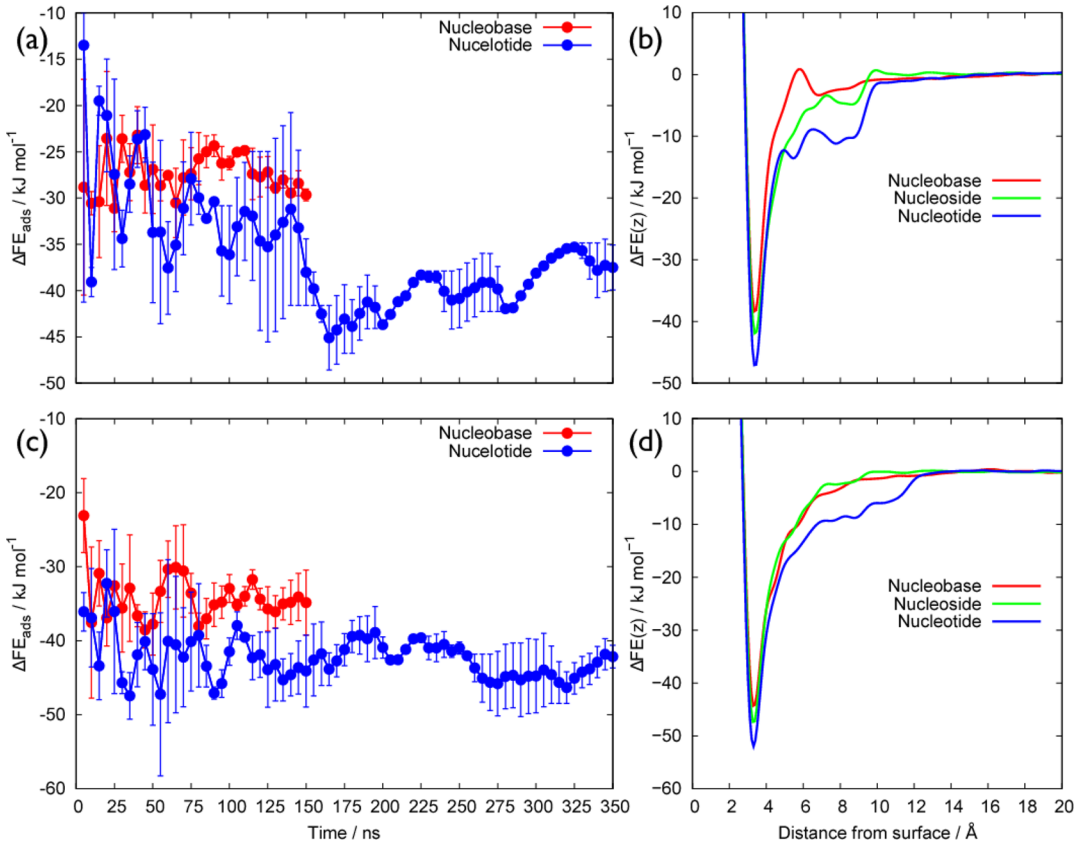

Figure 3. Free energy of adsorption as a function of time for the guanine nucleobase and nucleotide at (a) the aqueous C(0001) and (c) the aqueous Au(111) interfaces. Free energy profiles of the adsorption of the guanine nucleobase, nucleoside and nucleotide to (b) the aqueous C(0001) and (d) the aqueous Au(111) interfaces calculated from metadynamics simulations.

DOI: 10.1021/acs.langmuir.7b02480
Langmuir 2017, 33, 10193−10204

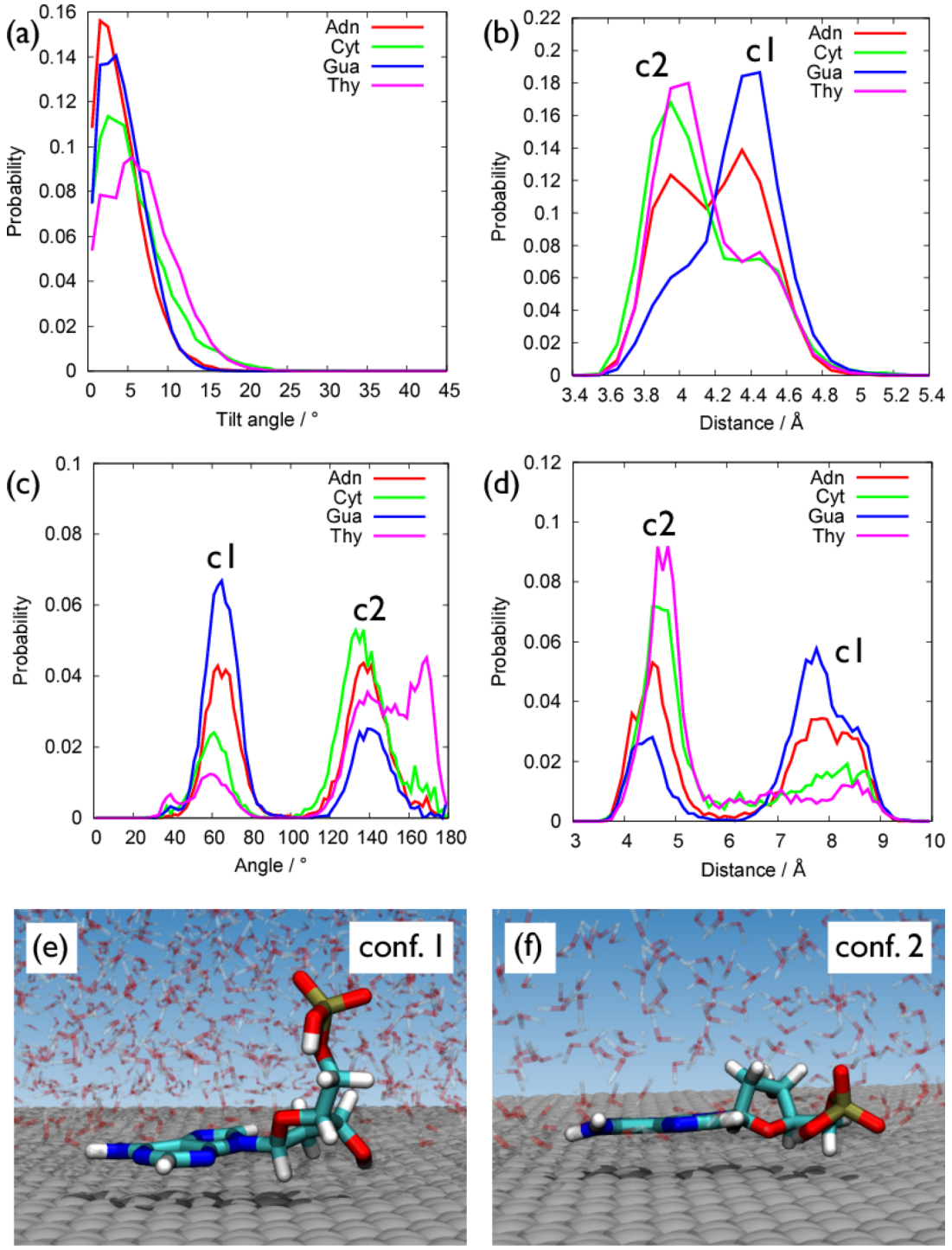

Figure 4. Structural data of nucleotides adsorbed at the aqueous C(0001) interface: (a–d) probability distributions of (a) the tilt angle of nucleobase ring with the C(0001) plane, (b) the distance between the center of mass of deoxyribose ring and the C(0001) interface, (c) the orientation of the deoxyribose ring with the interface normal, and (d) the distance between the phosphorus atom and the C(0001) interface. (e, f) Representative snapshots of deoxyadenosine monophosphate adsorbed at the aqueous C(0001) interface. The c1 and c2 notation in (b), (c), and (d) refers to conformations 1 and 2 shown in (e) and (f).

adsorption free energies; however, by 350 ns of metadynamics simulations the free energies were reasonably equilibrated, as indicated in Figure 3a and Figure S7. While the free energy profiles of the nucleotides differed from those of the nucleosides, the difference was not as pronounced as between the nucleosides and the nucleobases (Figure 3b and Figure S10). The predicted binding affinities of the nucleotides were stronger than those of the nucleosides. However, the relative ordering the nucleotides of G > A ≈ T > C remained the same, compared with the nucleosides. The presence of NaCl in the solvent did not appear to produce any meaningful difference in either the absolute adsorption free energies (Table S3) or the corresponding free energy profiles (Figures S8–S10). This finding is despite the fact that the density of salt ions within 15

DOI: 10.1021/acs.langmuir.7b02480
Langmuir 2017, 33, 10193–10204

Å of the substrate surface was greater than that in the bulk (Figure S12 shows the density profile of Na^+ and Cl^- in the C(0001) simulations).

As at the C(0001) interface, the adsorption free energies of the nucleobases at Au(111) reached a converged value relatively quickly, but the nucleosides and nucleotides required much longer metadynamics simulation times (see Figure 3c and Figures S5−S7). In contrast to C(0001), the adsorption free energy profiles of the nucleobases at the aqueous Au(111) interface (Figure 3d and Figure S7) showed only very minor barriers at the position corresponding with the first solvation layer. The adsorption free energies of the different nucleobases at the Au surface was less distinct than in the case of C(0001) (Figure S1 and Table S2). While the purines ($\Delta FE_{ads} \approx -35$ kJ mol^{-1}) adsorbed significantly more strongly than the pyrimidines ($\Delta FE_{ads} \approx -18$ kJ mol^{-1}), there was no significant difference in binding strength between A and T or G and C.

The significantly stronger adsorption of the purines remained in the case of the nucleosides and nucleotides (see Table 2 and Figures S6 and S7), with A and G adsorbing approximately equally as strongly. In the case of the pyrimidines, the adsorption of T was slightly weaker than that of C at the nucleoside/tide level, giving a relative ordering of G ≈ A > C > T. Unlike for the C(0001) interface, the adsorption free energy profiles of the nucleosides were not markedly broader than that of the nucleobases (Figure S11), although the addition of the phosphate group did induce some broadening. The depth of the free energy minimum increased with the size of the nucleic acid fragment.

The nucleobases adsorbed approximately parallel to the C(0001) or Au(111) surface (Figures S13 and S14). Our analysis suggests that the weaker the free energy of adsorption of the nucleobase, the more likely the nucleobase was to be tilted (slightly) with respect to the surface. The addition of the deoxyribose ring did not significantly affect the tilt angle of the aromatic ring with either substrate, and the sugar ring itself was most likely to be found ∼4.3−4.4 Å from the substrate surface (see Figures S15 and S16). At the C(0001) interface the dA, dG, and dT nucleosides were typically adsorbed with the vector between the center of mass of the sugar ring and the O4 atom oriented away from the surface. Cytosine differed from the other adsorbates in that there were four different orientational arrangements that were observed (all approximately equally likely). We suggest that the reason for these multiple adsorbed orientations for cytosine was due to the fact that as the most weakly adsorbing base, the aromatic ring competed with the deoxyribose ring for the most favorable surface-adsorbed contact point. For the other nucleic acids the aromatic ring dominated the interaction between the nucleoside and the surface. At the Au(111) interface the dominant adsorbed conformation of all four nucleosides featured the sugar ring oriented at an angle of ∼70° to the surface normal.

There were two adsorbed conformations of the nucleotides at the C(0001) interface, as shown in Figure 4. Both conformations featured the aromatic ring adsorbed flat at the surface, but with differing arrangements of the sugar ring and phosphate group. In conformation 1, the position/orientation of the deoxyribose ring was analogous to that of the nucleosides, while the phosphate group was located ∼8 Å from the surface, presented to the solution. In the case of conformation 2, the phosphate group was in direct contact with the C(0001) interface and the orientation vector of the deoxyribose ring was at an angle of ∼140° to the surface normal. The relative populations of the two conformations depended on the base. For G, conformation 1 was favored, for C and T conformation 2 was more likely, and for A the two conformations were approximately equally probable. At the Au(111) interface, the two adsorbed conformations of the nucleotides were analogous to those found at the C(0001) interface (see Figure S17). Again G showed a preference for a conformation with the phosphate group projected away from the surface, while T showed a preference for a conformation with the phosphate group close to the surface, and A and C did not show a preference for one conformation over the other.

Discussion. Before comparing the results of the SMFS experiments and metadynamics simulations, we discuss some of the limitations inherent to both techniques. Regarding SMFS, a key approximation lies in the choice of model used to infer ΔFE_{ads} from the measured adhesion forces. The present work used the model developed by Friddle, Noy, and De Yoreo,[36] where the loading rate of the experiment is related to the force required to desorb the adsorbate. The lower the loading rates used, the better the fit to obtain the force at the equilibrium state. Ideally, the plots of loading rates vs force (Figure 2 and Figure S4) should reach an asymptote at low loading rates. In practice, experimental constraints mean that such low loading rates are challenging to achieve. As a result, a non-negligible degree of uncertainty in the fit is an inevitable consequence. This is also the case when considering the potential error coming from using a single (average) force value, even for the cases where the histograms are not clearly peaked around a single value, that may correspond with a more complex adsorbate arrangement such as a quaduplex structure (*vide infra*).

In addition to the approximations inherent in the application of the Friddle, Noy, and De Yoreo model to the system, there are also uncertainties associated with the estimation of the effective stiffness of the PEG linker.[18] A further source of experimental uncertainty is that in contrast to the MD simulations, it is likely that the substrate was not pristine. Despite the considerable care taken to ensure the substrates were clean, the complete absence of surface contaminants is unlikely, and surface defects will be present. While the latter may not have an overly strong influence at the C(0001) interface, given that AFM imaging confirms that the surface is flat and clean, the Au(111) surface does possess a higher degree of surface roughness (Figure S2).

In considering the outcomes of the metadynamics simulations, possible limitations include the FFs used to describe the interfacial interactions, the challenges of comprehensively sampling the complex potential energy landscape (PEL) of the adsorbates, and the fact that out of practical necessity idealized substrate models were used. Regarding the conformational sampling, for complex adsorbates (with many internal degrees of freedom) it is currently thought that to obtain an accurate adsorption free energy it may be desirable to either use more than one collective variable in the metadynamics simulation[38] and/or combine metadynamics with an advanced sampling technique such as replica exchange MD.[16−19] Such strategies, however, can dramatically increase the computational cost of the simulations. Considering the plots of the free energy of adsorption vs time (Figures S5−S7), while ΔFE_{ads} quickly (within ∼70 ns) reached a stable value for the nucleobases, there was more variation for the nucleosides and nucleotides which might suggest that enhanced sampling strategies might accelerate convergence in these cases. However, it is worth

DOI: 10.1021/acs.langmuir.7b02480
Langmuir 2017, 33, 10193−10204

noting that the values of ΔFE_{ads} for C(0001) obtained for liquid water and for 0.16 kg mol^{-1} NaCl solution, which are independent runs, were consistent with each other. Regarding the veracity of the FFs, it is currently challenging to asses the accuracy of the FFs due to both the relative lack of relevant experimental data available for direct comparison and that both theory and experiment are invariably limited by approximations in their interpretation. In summary, it logically follows that direct like-for-like comparison between modeling and experiment in this field is rare and bound to a relatively large degree of uncertainty.[18]

While it is challenging to refine these interfacial FFs for the reasons described above, it is possible to make comparisons and rationalize the results with the help of other computational chemistry approaches. Comparison of the *in vacuo* adsorption energies, E_{ads} of the nucleobases obtained from the FFs and those obtained from density functional theory (DFT) calculations, with density functionals that account for weak interactions (a comparison is provided in Tables S1 and S2), indicate that not only do both FFs (Au(111) and C(0001)) reproduce the DFT-based trends in E_{ads}, but also that the agreement in the absolute values of E_{ads} is reasonable.

An additional challenge in drawing meaningful connections between the simulation and experimental data is that the experiments made use of 30 base ssDNA adsorbates, while the simulations were performed on individual nucleobases, nucleosides and nucleotides. Given that our simulation results suggested that different nucleotides yielded different proportions of the types of adsorbed conformation, the effect of neighboring nucleotides on the adhesion force of the ssDNA (and therefore their adsorption free energies) could vary with homo-oligomer. Thus, individual (free) nucleotides might assume adsorbed conformations that may not be relevant when part of an ssDNA oligomer.

For example, the adsorption free energy profiles of the nucleotides (and the nucleosides in the case of C(0001)) obtained from our metadynamics simulations exhibit a minimum of ∼−10 kJ mol^{-1} at a distance ∼8 Å from the surface. A representative snapshot of the adsorbed nucleotides corresponding with this minimum is provided in Figure 5, showing the deoxyribose and phosphate groups directly adsorbed at the substrate surface, with the nucleobase positioned above the first layer of bound water molecules. The SMFS measurements may not capture this local minimum (due to the aforementioned differences in the adsorption of a homo-oligomeric chain and the adsorption of a nucleotide) which could lead to discrepancies between the free energies estimated both by experiment and simulation. Moreover, the use of isolated nucleobases/tides/sides in our simulations will not capture effects arising from the formation of secondary structure in the ssDNA oligomers. Such secondary structure may influence the peeling force measured for the desorption of the ssDNA from the substrate. For dA_{30}, dC_{30}, and dT_{30} this is less likely to be a serious consideration but may be relevant for dG_{30}. Guanine-rich DNA sequences are known to support the formation of G-quartets and, in some cases, may form quadruplex structures.[39−41]

Given the varied sources of uncertainties for both approaches outlined above, in the following our results are first discussed considering only the trends in adsorption free energy expressed relative to cytosine, as shown in Figure 6. Discussion of the absolute values, which are all summarized in Table 3, will follow later, taking into account also the most relevant results reported in the experimental and theoretical literature.

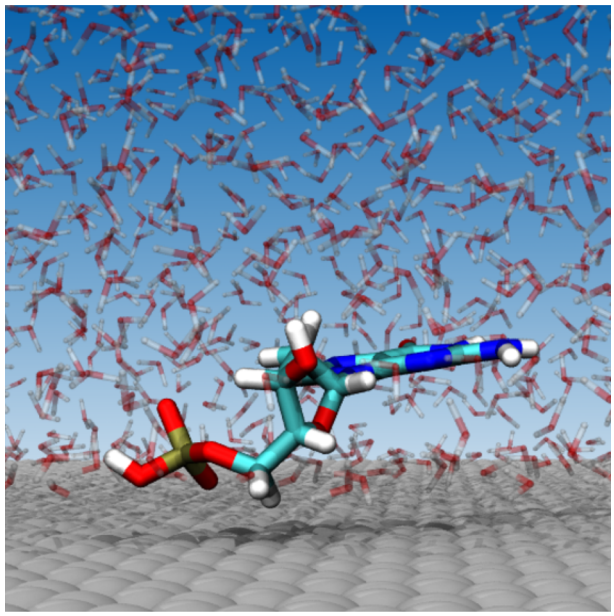

Figure 5. Snapshot of a representative conformation of the guanine nucleotide at the aqueous C(0001) interface, corresponding with the local minimum at ∼8 Å from the surface.

For the aqueous C(0001) interface, the trend comparison between the SMFS experiments and the metadynamics simulations is very reasonable (Figure 6a). Especially for the purines, the progression in adsorption free energies from nucleobase to nucleoside to nucleotide showed a steady improvement in the relative agreement between simulation and experiment. Both experiment and simulation indicated G to be the strongest binder and also suggested that A and T bound with approximately similar strengths.

For Au(111), large and in some case substantially overlapping experimental uncertainties between different adsorbates made the comparison less clear, with the larger discrepancy concerning the relative difference between G and T (evident in the simulations, absent in the experiments). Instead, the theoretical prediction that A adsorbed more strongly than C was well captured by the average experimental values.

An evident and interesting difference between C(0001) and Au(111) emerged from both experiments and simulations, namely, the stronger relative adsorption of A on Au(111) than on C(0001) with respect to the other bases. Our conformational analysis of the structures corresponding with the global minimum on the free energy surface suggested that both G and A assumed a planar adsorption geometry at this minimum, on both substrates. In this planar orientation, on the basis of van der Waals interactions only, we would expect the binding of G to be stronger than that of A (due to the presence of the carbonyl group on G, which is not featured in A). This is in fact the case for the C(0001) surface. However, our previous work indicates that the unprotonated nitrogen site (as found in the aromatic ring for both dA and dG) favors a strong interaction with the Au surface, even under aqueous conditions.[25] This interaction between the unprotonated nitrogen site on the ring can give rise to an adsorption geometry where the ring is oriented perpendicular to the surface (see Figure 6c). This type of interaction is not supported at the C(0001) interface.[13]

DOI: 10.1021/acs.langmuir.7b02480
Langmuir 2017, 33, 10193−10204

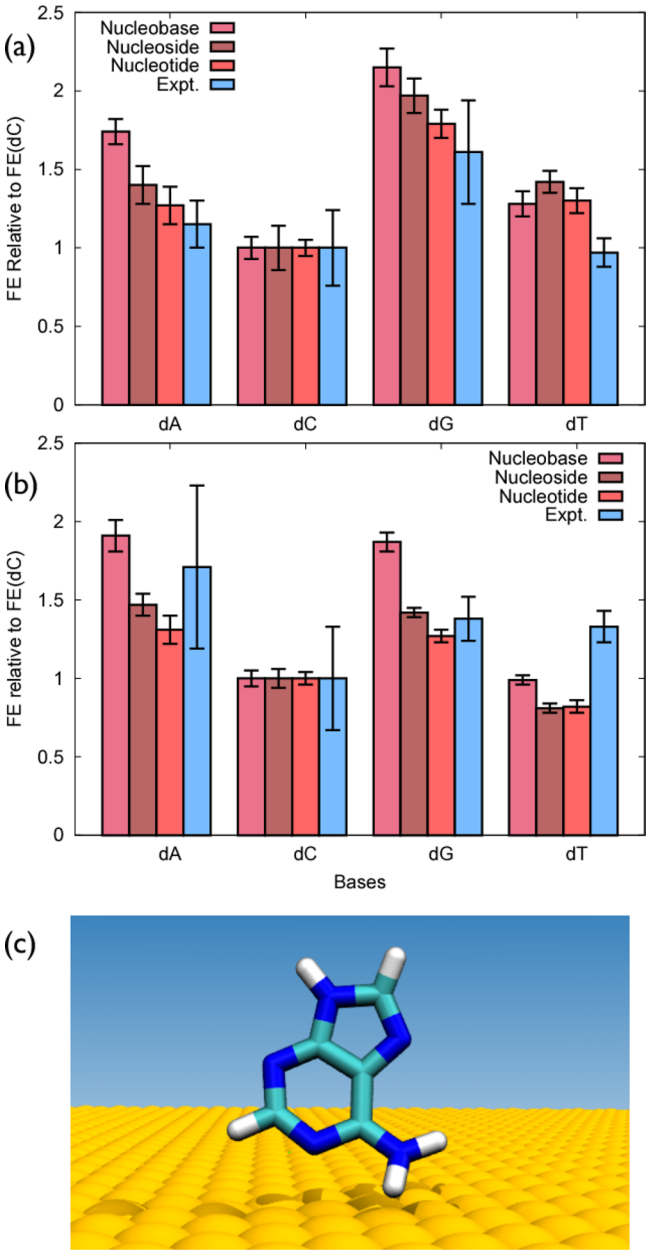

Figure 6. Relative free energies of the different adsorbates determined from both the metadynamics simulations as well as the experimental per-nucleotide free energy determined from single molecule force spectroscopy measurements: (a) for the aqueous C(0001) interface; (b) for the aqueous Au(111) interface. (c) The perpendicular adsorption geometry of the adenine nucleobase, which is not supported by guanine (see text for details). Water not shown for clarity.

Furthermore, we propose that steric hindrance (due to the presence of the carbonyl group on dG, which is not featured in dA) hindered this perpendicular adsorption geometry for dG, but not for dA. This additional adsorption geometry, present only for dA on Au(111), was also evident in the free energy profiles of A and G adsorbed at the Au(111) interface (Figure S11a,b). These profiles reveal an additional local minimum in the free energy profile for A, located ~6 Å from the Au surface, corresponding with this perpendicular geometry. Via our integration of the free energy profiles, this additional minimum in the free energy profile for the adenosine nucleobase contributes to the stronger binding affinity of A at the Au(111) interface compared with G.

As far as the absolute values of the adsorption free energy are concerned, for all four bases on both substrates the metadynamics simulations showed a progressive increase from the nucleobase to the nucleoside to the nucleotide (Table 2). However, as Figure 6 indicates, the presence of the deoxyribose and phosphate groups appeared in general to reduce the relative differences between the different bases.

To provide further context for our experimental and simulation data, Table 3 summarizes the results of previously published studies, both experimental and theoretical, including previous SMFS experiments reported for homo-oligonucleotides adsorbed on graphitic[34,35] or gold[42] substrates. We emphasize here that measurements of adhesion forces can only be used as a viable way to estimate binding strengths if they are interpreted according to kinetics models such as e.g. the model proposed by Friddle, Noy, and De Yoreo,[36] used in the current study. However, all models attempting to extract equilibrium quantities from nonequilibrium experiments must necessarily rely on assumptions, and their validity with respect to the system under investigation may be limited.

An alternative experimental approach to SMFS is isothermal titration calorimetry (ITC), as used by Ranganathan et al.[43] However, the use of ITC to infer molecule−surface binding affinities from the measured heats of adsorption is a similarly fraught process. As with SMFS, ITC also requires assumptions to inform an appropriate binding site model, i.e., to determine parameters such as the cooperativity, *c*, which are pivotal to extracting meaningful findings from the raw data.[44] In addition, Ranganathan et al. used both graphene oxide (GO) and reduced GO nanoflakes in aqueous solution as their binding substrate. Therefore, these substrates may differ significantly from HOPG/pristine graphite in terms of their surface chemistry. Moreover, the potential aggregation of the reduced GO nanoflakes in solution might also give rise to significant differences in measured ΔFE_{ads}, compared with a pristine HOPG aqueous interface.

In light of all of these uncertainties, it is understandable that differences can be found in the absolute ΔFE_{ads} values between the various experimental and simulation data. Despite this, the degree of consistency between our data and that of Manohar et al.[34] and Iliafar et al.[45] is quite encouraging. In terms of the trend on graphitic substrates, there is reasonable agreement between our work and the ITC-based estimates of Ranganathan et al.,[43] with both suggesting the purines as stronger binders than the pyrimidines. In contrast, Iliafar et al. reported a rank ordering in binding strengths of dT ≈ dA > dG ≈ dC. However, the authors found it particularly challenging to estimate a value for poly dG, which was attributed to the greater propensity of guanine to form stable secondary structures (*vide supra*). For the Au(111) interface, both the results of the current work and the SMFS study reported by Bano et al.[42] suggested dA as the strongest binder and with dG and dC featuring approximately equal binding strengths. However, while our data estimate the binding of dT as similar to that of dG/dC, Bano et al. reported dT to be the relatively weakest binder by a considerable margin.

In terms of previous simulation-based estimates of adsorption free energies of DNA fragments on graphitic substrates under aqueous conditions, in agreement with the present work, previous studies using the AMBER99 FF suggested a trend of G > A ≈ T > C for both the nucleobases

DOI: 10.1021/acs.langmuir.7b02480
Langmuir 2017, 33, 10193−10204

Table 3. Summary of Estimated Free Energies of Adsorption, ΔFE_{ads}, of DNA Fragments to Aqueous Graphitic and Gold Interfaces, Including Estimates from Previous Work Both Experimental and Simulation

				ΔFE_{ads} (kJ mol^{-1})			
substrate	reference	method	adsorbate[a]	dA	dC	dG	dT
graphitic	present work	SMFS	O	−38 ± 5	−32 ± 3	−53 ± 11	−33 ± 8
	Iliafar[34,35]	SMFS	O	−41.4 ± 2.1	−31.4 ± 3.3	−34.7 ± 0.8	−47.3 ± 3.3
	Ranganathan[43b]	ITC	NS	−26.0 ± 0.2	−22.8 ± 0.2	−26.4 ± 0.5	−21.6 ± 1.5
	present work	Sim	NB	−22.5 ± 1.0	−12.9 ± 0.9	−27.7 ± 1.6	−16.5 ± 1.0
	present work	Sim	NS	−25.2 ± 2.1	−18.0 ± 2.5	−35.4 ± 1.9	−25.6 ± 1.3
	present work	Sim	NT	−27.1 ± 2.5	−21.4 ± 1.0	−38.3 ± 2.0	−27.9 ± 2.1
	Johnson[46c]	Sim	NB	−35.1 ± 1.3	−26.8 ± 1.7	−43.1 ± 1.7	−32.2 ± 1.7
	Ranganathan[43d]	Sim	NS	−58	−46	−67	−52
	Ranganathan[43e]	Sim	NS	−38	−29	−42	−29
	Ranganathan[43f]	Sim	NS	−24	−20	−26	−20
	Shi[47]	Sim	O	−113.0	−100.4	−125.5	−108.8
gold	present work	SMFS	O	−36 ± 11	−21 ± 7	−29 ± 3	−28 ± 2
	Bano[42g]	SMFS	O	−23.6 ± 0.1	−13.3 ± 0.1	−13 ± 0.1	−7.8 ± 0.1
	present work	Sim	NB	−35.4 ± 1.8	−18.5 ± 1.0	−34.6 ± 1.1	−18.3 ± 0.5
	present work	Sim	NS	−39.4 ± 1.8	−26.8 ± 1.7	−38.1 ± 0.9	−21.8 ± 0.9
	present work	Sim	NT	−45.7 ± 3.1	−34.9 ± 1.3	−44.4 ± 1.3	−28.6 ± 1.5

[a]Nucleobase (NB), nucleoside (NS), nucleotide (NT), or oligomer (O). [b]On reduced GO. [c]On (11,0) CNT, AMBER99 parameters. [d]On graphene, AMBER99 parameters. [e]On graphene, Chen−Garcia parameters. [f]On graphene, revised parameters. [g]On gold-coated silicon wafers.

to (11,0) CNTs[46] and the nucleosides to graphene.[43] However, the absolute ΔFE_{ads} values reported in these studies were substantially greater than those obtained in the current study. In contrast, the absolute values of ΔFE_{ads} obtained using the Chen−Garcia[48] or Ranganathan parameters were both lower and yielded a binding trend of G > A > T ≈ C.[43] Shi et al. attempted to use steered MD simulations of homo-oligonucleotide ssDNA to obtain ΔFE_{ads} values; however, the extremely high pulling rate used in this work means that these values are highly likely to be severe overestimates.

Using thermodynamic integration, Manohar et al. predicted a ΔFE_{ads} of −46.9 kJ mol^{-1} for the thymine nucleotide at the aqueous graphite interface using the CHARMM27 FF parameters. When comparing the free energies obtained from their ITC experiments against those obtained from simulation, Ranganathan et al. suggested that the AMBER99 parameters, and, to a lesser extent, the Chen−Garcia parameters, overbound DNA bases to graphitic substrates.[43] While bearing in mind the uncertainties outlined above, the experimental estimates consistently yielded lower absolute values of ΔFE_{ads} compared with those obtained with the unmodified AMBER99 FF parameters. Therefore, we suggest that simulation data generated by modeling graphitic surfaces as uncharged atoms with the unmodified AMBER99FF C sp^2 LJ parameters should be viewed with caution.

At the Au(111) aqueous interface, Rosa et al.[12] used the GolPDNA-AMBER FF to determine the adsorption free energy profile of the cytosine nucleobase, which featured a minimum of −10.9 kJ mol^{-1}, compared with the value of −26.8 kJ mol^{-1} for the current work. We emphasize here that Rosa et al. reported the well depth of the FE profile only and did not integrate their profile to calculate the adsorption free energy, while our value was obtained by integrating our FE profile, which means we cannot make a direct comparison between these two values. The GolPDNA-AMBER FF also yielded a much more pronounced barrier between the direct and solvent-separated conformations compared with our profiles generated using GolP-CHARMM. Therefore, due to the presence of this higher barrier, we anticipate that integration of the FE profile reported by Rosa et al. would produce an absolute value of FE_{ads} that would be lower than our value.

Finally, the effect of the presence of salt ions in solution on the adsorption free energy is another open question. Our simulation data suggested that the adsorption strengths predicted for the 0.16 mol kg^{-1} NaCl solution ΔFE_{ads} of individual DNA fragments at the C(0001) interface did not differ substantially with those binding strengths calculated in liquid water. This result is consistent with the findings of Ranganathan et al.,[43] who observed no effect on ΔFE_{ads} in the presence 1 mol kg^{-1} KCl solution in their simulations. Moreover, in the experimental study reported by Iliafar et al.,[45] the magnitude of the average peeling forces appeared to be broadly insensitive to varying salt concentration in solution. However, other studies have reported that salt effects may influence the binding strength of DNA oligomers.[7,49]

CONCLUSIONS

In conclusion, our combined experimental and modeling approach, in partnership with careful analysis, provides a valuable and versatile strategy for quantifying and interpreting the binding traits of nucleic acid/materials interfaces. The complexity of such biohybrid interfaces is immediately evident by the large scattering of adsorption free energy values currently available in the literature. This calls for further in-depth studies devoted, in particular, to comparing several different theoretical and experimental methods and assessing the validity of the model-specific assumptions therein.

In the present work, the binding strengths of nucleic acid fragments on aqueous C(0001) and Au(111) were determined experimentally using single molecule force spectroscopy measurements and were predicted via all-atom metadynamics simulations based on polarizable force fields. We found reasonable consistency between the experimental and modeling data. However, the consideration of several limitations and approximations, inherent to both the experimental interpretation of the adhesion force data and the calculation of the metadynamics-based free energies, hindered a clear-cut comparison of relative binding strengths, particularly for gold.

DOI: 10.1021/acs.langmuir.7b02480
Langmuir 2017, 33, 10193−10204

On C(0001), our simulations predicted a binding trend of dG > dA ≈ dT > dC, which was broadly consistent with the experimental data. At the aqueous Au(111) interface, the relative binding strength of adenine was significantly increased—a fact that we could rationalize via analysis of the binding conformations predicted by the simulations. This led to a slightly different adsorption trend on Au(111), namely dG ≈ dA > dT ≈ dC. In agreement with several previous studies, our simulations suggested little to no influence of salt concentration on the predicted binding strengths. Our modeling data also provided insights into the adsorption geometries at these substrates, as a function of nucleic acid fragment size, by considering binding of the nucleobases, nucleosides, and nucleotides. In general, the binding trends predicted for both substrates was consistent across these three levels of fragment size.

■ ASSOCIATED CONTENT

Supporting Information

The Supporting Information is available free of charge on the ACS Publications website at DOI: 10.1021/acs.langmuir.7b02480.

Figures S1−S17 and Tables S1−S3 (PDF)

■ AUTHOR INFORMATION

Corresponding Authors

*E-mail: colombi@hmi.uni-bremen.de (L.C.C.).
*E-mail: tiffany.walsh@deakin.edu.au (T.R.W.).

ORCID

Zak E. Hughes: 0000-0003-2166-9822
Gang Wei: 0000-0002-3838-8659
Lucio Colombi Ciacchi: 0000-0003-1444-9733
Tiffany R. Walsh: 0000-0002-0233-9484

Notes

The authors declare no competing financial interest.

■ ACKNOWLEDGMENTS

This research was supported in part by the Asian Office of Aerospace Research and Development (AOARD), grant FA2386-16-1-4053. We are grateful for computational resources provided by the National Computational Infrastructure (NCI), which is supported by the Australian Government. The authors also thank the Victorian Life Sciences Computation Initiative (VLSCI) for computational resources. T.R.W. thanks **veski** for research funding and an Innovation Fellowship. K.L.M.D. thanks the Australian Government for an APA PhD scholarship. G.W. and L.C.C. acknowledge support from the Deutsche Forschungsgemeinschaft (DFG) under grants WE 5837/1-1 (G.W.) and CI 144/2 (L.C.C.). G.W. thanks R. H. Meißner for calculating the spring constant of the PEG linker, K_{PEG}.

■ REFERENCES

(1) Liu, Y.; Dong, X.; Chen, P. Biological and chemical sensors based on graphene materials. *Chem. Soc. Rev.* **2012**, *41*, 2283.
(2) Li, Q.; Zhang, T.; Pan, Y.; Colombi Ciacchi, L.; Xu, B.; Wei, G. AFM-based Force Spectroscopy for Bioimaging and Biosensing. *RSC Adv.* **2016**, *6*, 12893−12912.
(3) Webb, J. A.; Bardhan, R. Emerging advances in nanomedicine with engineered gold nanostructures. *Nanoscale* **2014**, *6*, 2502.
(4) Dickerson, M. B.; Sandhage, K. H.; Naik, R. R. Protein- and Peptide-Directed Syntheses of Inorganic Materials. *Chem. Rev.* **2008**, *108*, 4935−4978.
(5) Care, A.; Bergquist, P. L.; Sunna, A. Solid-binding peptides: smart tools for nanobiotechnology. *Trends Biotechnol.* **2015**, *33*, 259−268.
(6) Wei, G.; Steckbeck, S.; Köppen, S.; Colombi Ciacchi, L. Label-free biosensing with single-molecule force spectroscopy. *Chem. Commun.* **2013**, *49*, 3239.
(7) Wei, G.; Li, Q.; Steckbeck, S.; Colombi Ciacchi, L. Direct force measurements on peeling heteropolymer ssDNA from a graphite surface using single-molecule force spectroscopy. *Phys. Chem. Chem. Phys.* **2014**, *16*, 3995.
(8) Bedford, N. M.; Hughes, Z. E.; Tang, Z.; Li, Y.; Briggs, B. D.; Ren, Y.; Swihart, M. T.; Petkov, V. G.; Naik, R. R.; Knecht, M. R.; Walsh, T. R. Sequence-Dependent Structure/Function Relationships of Catalytic Peptide-Enabled Gold Nanoparticles Generated under Ambient Synthetic Conditions. *J. Am. Chem. Soc.* **2016**, *138*, 540−548.
(9) Ozboyaci, M.; Kokh, D. B.; Corni, S.; Wade, R. C. Modeling and Simulation of Protein-surface Interactions: Achievements and Challenges. *Q. Rev. Biophys.* **2016**, *49*, 1−45.
(10) Iori, F.; Di Felice, R.; Molinari, E.; Corni, S. GolP: An atomistic force-field to describe the interaction of proteins with Au(111) surfaces in water. *J. Comput. Chem.* **2009**, *30*, 1465−1476.
(11) Wright, L. B.; Rodger, P. M.; Corni, S.; Walsh, T. R. GolP-CHARMM: First-Principles Based Force-fields for the Interaction of Proteins with Au(111) and Au(100). *J. Chem. Theory Comput.* **2013**, *9*, 1616−1630.
(12) Rosa, M.; Corni, S.; Di Felice, R. Enthalpy-Entropy Tuning in the Adsorption of Nucleobases at the Au(111) Surface. *J. Chem. Theory Comput.* **2014**, *10*, 1707−1716.
(13) Hughes, Z. E.; Tomásio, S. M.; Walsh, T. R. Efficient simulations of the aqueous bio-interface of graphitic nanostructures with a polarisable model. *Nanoscale* **2014**, *6*, 5438−5448.
(14) Wei, Y.; Latour, R. A. Determination of the Adsorption Free Energy for Peptide-Surface Interactions by SPR Spectroscopy. *Langmuir* **2008**, *24*, 6721−6729.
(15) Cohavi, O.; Reichmann, D.; Abramovich, R.; Tesler, A. B.; Bellapadrona, G.; Kokh, D. B.; Wade, R. C.; Vaskevich, A.; Rubinstein, I.; Schreiber, G. A Quantitative, Real-Time Assessment of Binding of Peptides and Proteins to Gold Surfaces. *Chem. - Eur. J.* **2011**, *17*, 1327−1336.
(16) Schneider, J.; Colombi Ciacchi, L. Specific Material Recognition by Small Peptides Mediated by the Interfacial Solvent Structure. *J. Am. Chem. Soc.* **2012**, *134*, 2407−2413.
(17) Mijajlovic, M.; Penna, M. J.; Biggs, M. J. Free Energy of Adsorption for a Peptide at a Liquid/Solid Interface via Non-equilibrium Molecular Dynamics. *Langmuir* **2013**, *29*, 2919−2926.
(18) Meißner, R. H.; Wei, G.; Colombi Ciacchi, L. Estimation of the free energy of adsorption of a polypeptide on amorphous SiO_2 from molecular dynamics simulations and force spectroscopy experiments. *Soft Matter* **2015**, *11*, 6254−6265.
(19) Wright, L. B.; Palafox-Hernandez, J. P.; Rodger, P. M.; Corni, S.; Walsh, T. R. Facet selectivity in gold binding peptides: exploiting interfacial water structure. *Chem. Sci.* **2015**, *6*, 5204−5214.
(20) Hoefling, M.; Iori, F.; Corni, S.; Gottschalk, K.-E. Interaction of Amino Acids with the Au(111) Surface: Adsorption Free Energies from Molecular Dynamics Simulations. *Langmuir* **2010**, *26*, 8347−8351.
(21) Barducci, A.; Bussi, G.; Parrinello, M. Well-tempered metadynamics: a smoothly converging and tunable free-energy method. *Phys. Rev. Lett.* **2008**, *100*, 020603.
(22) Li, Q.; Michaelis, M.; Wei, G.; Colombi Ciacchi, L. A novel aptasensor based on single-molecule force spectroscopy for highly sensitive detection of mercury ions. *Analyst* **2015**, *140*, 5243−5250.
(23) Hutter, J. L.; Bechhoefer, J. Calibration of Atomic-Force Microscope Tips. *Rev. Sci. Instrum.* **1993**, *64*, 1868−1873.
(24) Hughes, Z. E.; Walsh, T. R. What makes a good graphene-binding peptide? Adsorption of amino acids and peptides at aqueous graphene interfaces. *J. Mater. Chem. B* **2015**, *3*, 3211−3221.

DOI: 10.1021/acs.langmuir.7b02480
Langmuir 2017, 33, 10193−10204

(25) Hughes, Z. E.; Kochandra, R.; Walsh, T. R. Facet-Specific Adsorption of Tripeptides at Aqueous Au Interfaces: Open Questions in Reconciling Experiment and Simulation. *Langmuir* **2017**, *33*, 3742−3754.
(26) MacKerell, A. D., Jr.; Bashford, D.; Bellott, M.; Dunbrack, R. L., Jr.; Evanseck, J. D.; Field, M. J.; Fischer, S.; Gao, J.; Guo, H.; Ha, S.; et al. All-atom empirical potential for molecular modeling and dynamics studies of proteins. *J. Phys. Chem. B* **1998**, *102*, 3586−3616.
(27) Jorgensen, W. L.; Chandrasekhar, J.; Madura, J. D.; Impey, R. W.; Klein, M. L. Comparison of simple potential functions for simulating liquid water. *J. Chem. Phys.* **1983**, *79*, 926−935.
(28) Neria, E.; Fischer, S.; Karplus, M. Simulation of activation free energies in molecular systems. *J. Chem. Phys.* **1996**, *105*, 1902−1921.
(29) Hess, B.; Kutzner, C.; Van Der Spoel, D.; Lindahl, E. GROMACS 4: Algorithms for Highly Efficient, Load-Balanced, and Scalable Molecular Simulation. *J. Chem. Theory Comput.* **2008**, *4*, 435−447.
(30) Bonomi, M.; Branduardi, D.; Bussi, G.; Camilloni, C.; Provasi, D.; Raiteri, P.; Donadio, D.; Marinelli, F.; Pietrucci, F.; Broglia, R. A. PLUMED: A portable plugin for free-energy calculations with molecular dynamics. *Comput. Phys. Commun.* **2009**, *180*, 1961−1972.
(31) Darden, T.; York, D.; Pedersen, L. Particle Mesh Ewald - an N.Log(N) Method for Ewald Sums in Large Systems. *J. Chem. Phys.* **1993**, *98*, 10089−10092.
(32) Nosé, S. A unified formulation of the constant temperature molecular dynamics methods. *J. Chem. Phys.* **1984**, *81*, 511−519.
(33) Hoover, W. Canonical dynamics: Equilibrium phase-space distributions. *Phys. Rev. A: At., Mol., Opt. Phys.* **1985**, *31*, 1695−1697.
(34) Manohar, S.; Mantz, A. R.; Bancroft, K. E.; Hui, C.-Y.; Jagota, A.; Vezenov, D. V. Peeling Single-Stranded DNA from Graphite Surface to Determine Oligonucleotide Binding Energy by Force Spectroscopy. *Nano Lett.* **2008**, *8*, 4365−4372.
(35) Iliafar, S.; Wagner, K.; Manohar, S.; Jagota, A.; Vezenov, D. Quantifying Interactions between DNA Oligomers and Graphite Surface Using Single Molecule Force Spectroscopy. *J. Phys. Chem. C* **2012**, *116*, 13896−13903.
(36) Friddle, R. W.; Noy, A.; De Yoreo, J. J. *Proc. Natl. Acad. Sci. U. S. A.* **2012**, *109*, 13573−13578.
(37) Le, D.; Kara, A.; Schröder, E.; Hyldgaard, P.; Rahman, T. S. Physisorption of nucleobases on graphene: a comparative van der Waals study. *J. Phys.: Condens. Matter* **2012**, *24*, 424210.
(38) Bellucci, L.; Corni, S. Interaction with a Gold Surface Reshapes the Free Energy Landscape of Alanine Dipeptide. *J. Phys. Chem. C* **2014**, *118*, 11357−11364.
(39) Reshetnikov, R.; Golovin, A.; Spiridonova, V.; Kopylov, A.; Sponer, J. Structural Dynamics of Thrombin-Binding DNA Aptamer d(GGTTGGTGTGGTTGG) Quadruplex DNA Studied by Large-Scale Explicit Solvent Simulations. *J. Chem. Theory Comput.* **2010**, *6*, 3003−3014.
(40) Rebič, M.; Laaksonen, A.; Sponer, J.; Uličný, J.; Mocci, F. Molecular Dynamics Simulation Study of Parallel Telomeric DNA Quadruplexes at Different Ionic Strengths: Evaluation of Water and Ion Models. *J. Phys. Chem. B* **2016**, *120*, 7380−7391.
(41) Grunenberg, J.; Barone, G.; Spinello, A. The Right Answer for the Right Electrostatics: Force Field Methods Are Able to Describe Relative Energies of DNA Guanine Quadruplexes. *J. Chem. Theory Comput.* **2014**, *10*, 2901−2905.
(42) Bano, F.; Sluysmans, D.; Wislez, A.; Duwez, A.-S. Unraveling the complexity of the interactions of DNA nucleotides with gold by single molecule force spectroscopy. *Nanoscale* **2015**, *7*, 19528−19533.
(43) Ranganathan, S. V.; Halvorsen, K.; Myers, C. A.; Robertson, N. M.; Yigit, M. V.; Chen, A. A. Complex Thermodynamic Behavior of Single-Stranded Nucleic Acid Adsorption to Graphene Surfaces. *Langmuir* **2016**, *32*, 6028−6034.
(44) Brown, A. Analysis of Cooperativity by Isothermal Titration Calorimetry. *Int. J. Mol. Sci.* **2009**, *10*, 3457−3477.
(45) Iliafar, S.; Mittal, J.; Vezenov, D.; Jagota, A. Interaction of Single-Stranded DNA with Curved Carbon Nanotube is Much Stronger than with Flat Graphite. *J. Am. Chem. Soc.* **2014**, *136*, 12947−12957.
(46) Johnson, R. R.; Johnson, A. T. C.; Klein, M. L. The nature of DNA-base-carbon-nanotube interactions. *Small* **2010**, *6*, 31−34.
(47) Shi, X.; Kong, Y.; Zhao, Y.; Gao, H. Molecular dynamics simulation of peeling a DNA molecule on substrate. *Acta Mech. Sin.* **2005**, *21*, 249−256.
(48) Chen, A. A.; Garcia, A. E. High-resolution reversible folding of hyperstable RNA tetraloops using molecular dynamics simulations. *Proc. Natl. Acad. Sci. U. S. A.* **2013**, *110*, 16820−16825.
(49) Wu, M.; Kempaiah, R.; Huang, P.-J. J.; Maheshwari, V.; Liu, J. Adsorption and Desorption of DNA on Graphene Oxide Studied by Fluorescently Labeled Oligonucleotides. *Langmuir* **2011**, *27*, 2731−2738.

DOI: 10.1021/acs.langmuir.7b02480
Langmuir 2017, 33, 10193−10204